DETAILED MODELING ANALYSIS FOR SOOT FORMATION AND RADIATION IN MICROGRAVITY GAS JET DIFFUSION FLAMES

Jerry C. Ku and Li Tong, Department of Mechanical Engineering, Wayne State University, Detroit, Michigan 48202
and
Paul S. Greenberg, Microgravity Combustion Branch, NASA/Lewis, Cleveland, Ohio 44135

Introduction

Radiation heat transfer in combustion systems has been receiving increasing interest (ref. 1). In the case of hydrocarbon fuels, a significant portion of the radiation comes from soot particles, justifying the need for detailed soot formation model and radiation transfer calculations. For laminar gas jet diffusion flames, results from this project (4/1/91-8/22/95) and another NASA study (ref. 2) show that flame shape, soot concentration, and radiation heat fluxes are substantially different under microgravity conditions.

Our emphasis is on including detailed soot transport models and a detailed solution for radiation heat transfer, and on coupling them with the flame structure calculations. In this paper, we will discuss the following three specific areas:

1. Comparing two existing soot formation models, and identifying possible improvements.

2. A simple yet reasonably accurate approach to calculating total radiative properties and/or fluxes over the spectral range.

3. Investigating the convergence of iterations between the flame structure solver and the radiation heat transfer solver.

Modeling of Jet Diffusion Flame Structure

The structure of turbulent jet diffusion flames is modeled using the Favre-averaged equations for conservation of mass, momentum, and mixture fraction. A conserved scalar approach (refs. 3, 4 and 5) with an assumed probability density function (pdf) and a k-ε-g turbulence model (ref. 6) are used. All governing equations can be written in a general form as (ref. 7)

$$\frac{\partial}{\partial x}(\bar{\rho}\tilde{u}\phi) + \frac{1}{r}\frac{\partial}{\partial r}(r\bar{\rho}\tilde{v}\phi) = \frac{1}{r}\frac{\partial}{\partial r}\left(r\mu_{\mathit{eff},\phi}\frac{\partial\phi}{\partial r}\right) + S_{\phi} \ , \tag{1}$$

where $\phi = 1$, $\tilde{u}$ (velocity), $\tilde{f}$ (mixture fraction), k (kinetic energy), ε (dissipation), or g (variance on f). Details for $\mu_{\mathit{eff},\phi}$ (effective viscosity), S_{ϕ} (source term) and assumptions can be found in references. Buoyancy effects are considered in mean flow only, neglecting buoyancy-turbulence interactions. For laminar flames, Eq. (1) is simplified accordingly.

The system represented by Eq. (1) is solved using the block-tridiagonal code of Chen et al. (ref. 8). State relationships are constructed from equilibrium calculations using STANJAN (ref. 9) to allow chemical reactions to be decoupled from flow calculations. More accurate laminar flamelet approaches (refs. 10 and 11) may be considered in the future.

Modeling of Soot Formation and Oxidation

We have considered two sets of soot formation and oxidation models. Both describe the transport of soot particles based on Eq. (1). The two-equation model developed by Moss, Syed and Stewart (refs. 12 and 13) is based on number density (N) and volume fraction (f_v), and the two respective source terms are

$$S_{\hat{N}} = \bar{\alpha} - \bar{\beta}\bar{\rho}^2\hat{N}^2 - n_0^{1/3}\bar{\chi}\bar{\rho}\hat{f}_v^{-1/3}\hat{N}^{4/3} \ , \quad \phi = \hat{N} \equiv \frac{N}{\rho n_0} \ ; \tag{2}$$

$$S_{\hat{f}_v} = n_0^{1/3}(\bar{\gamma}-\bar{\chi})\bar{\rho}\hat{f}_v^{2/3}\hat{N}^{1/3} + C_\delta\bar{\alpha} \ , \quad \phi = \hat{f}_v \equiv \frac{\rho_s f_v}{\rho} \ ; \tag{3}$$

where $n_0 = 6\times10^{26}$ is Avogadro's number and ρ_s is the mass density of soot (typically 1.8-2.0 g/cm³). Rate-equations of Arrhenius type are used to model nucleation (α), growth (β), coagulation (γ) and oxidation (χ), in terms of flame temperature T, mixture density $\bar{\rho}$, fuel and gas mole fractions, and activation temperatures. Existing soot oxidation

models (refs. 14 and 15) are modified to include oxidation by both O_2 and OH. Details on model coefficients and the oxidation model can be found in ref. 16. For laminar flames, both Eq. (1) and rate-equation models are simplified, with the addition of a radial thermophoretic velocity $v_t = -.054(v/T)(\partial T/\partial r)$.

Another model is a one-equation model, based on volume fraction only, developed by Khan et al. (refs. 17 and 18). This model characterizes soot formation by an Arrhenius-type equation, and the corresponding source term is

$$S_{\hat{f}_v} = C_k P_{fu}\varphi^3\left(\frac{\rho}{\rho_s}\right)\exp\left(-\frac{E_s}{RT}\right) \ , \quad \phi = \hat{f}_v \equiv \frac{\rho_s f_v}{\rho} \ ; \tag{4}$$

where $C_k = 16.8$ kg/Nms, P_{fu} denotes the partial pressure of unburned fuel, φ is the local fuel/air equivalence ratio, and $E_s = 40000$ cal/mole is the activation energy. The soot oxidation model of Lee et al. (ref. 19) is adopted, which is similar to Eq. (4), except with $\varphi^3(\rho/\rho_s)$ replaced by $\hat{f}_v/\sqrt{T}$.

The model by Khan et al. is simpler, but it may not be as physically sound as that by Moss et al., since it does not include such mechanisms as coagulation which causes decreasing number density under constant volume fraction.

Solution for Flame Radiation Heat Transfer

Although it plays an important role, radiation heat transfer is usually not treated in detail in combustion analyses due to such difficulties as the accuracy and computational efficiency of various solutions for the radiative transfer equation (ref. 20), the coupling of radiation and combustion solvers, the accuracy of spectral radiative properties, and efficient methods for integrating fluxes and other results over the spectral range.

We chose the recently developed YIX method (refs. 21 and 22) for calculating the radiative heat flux $\vec{q}_{rad}$ and its divergence. The YIX method is a numerical approach for solving the integral formulation of the radiative transfer equation by reducing the order of the multiple distance-angular integrals. The name YIX comes from the shape of the pattern of integration points for three, two, and four angular directions. One important attribute of this method is that these integration points can be pre-calculated and stored, significantly reducing computational time. For multi-dimensional geometries, discrete ordinate sets are used for angular quadratures. Although computationally quite intensive, the YIX method has proven to be very accurate and suitable for nonhomogeneous media (refs. 23 and 24). Simplified models such as a fixed percentage of local heat loss from equilibrium everywhere, a temperature modified from that under equilibrium as $T = T_{eq}[1 - \beta(T_{eq}/T_{eq,max})^4]$ (ref. 14), and a heat "sink" as $S_\phi = -\varepsilon\sigma(T^4 - T_\infty^4)/\ell$ (ref. 25) have each been tested and found inaccurate. We derived the spherical harmonics (P_N) approximate solution for non-homogeneous media following ref. 26, but found it numerically unstable in optically-thin regions.

The radiation solver is coupled to the flame structure solver through the energy equation. For diffusion flames, the energy equation takes the same form as Eq. (1), with $\phi = H$ (total enthalpy) and $S_\phi = -\nabla \cdot \vec{q}_{rad}$, and the latter can be calculated from a solution for the radiative transfer equation. These two solvers, both depending on the temperature, are computationally incompatible. The solver for flame structure, soot transport, and the energy equation solves parabolic differential equations of Eq. (1) type. The solver for radiative transfer, YIX or otherwise, is inherently not parabolic, since radiation is an "integral" phenomenon over all distances and solid angles. We chose an iterative approach and used temperature as the convergence criterion. The iteration starts with the flame structure solver and an initial guess of $S_\phi = -\varepsilon\sigma(T^4 - T_\infty^4)/\ell$ to calculate velocities, gas and soot concentrations, density, and flame temperature. The resulting temperature is used for calculating $\nabla \cdot \vec{q}_{rad}$ from the YIX solver. The resulting $\nabla \cdot \vec{q}_{rad}$ is substituted back into the structure solver to update (by averaging the two latest runs) velocities, concentrations, density, and temperature. This process is then repeated until a convergence on the temperature is accomplished between two subsequent iterations ($\Delta T/T < 0.002$). The turbulence-radiation interactions, which have been shown to be significant by Gore et al. (ref. 27), will be included in the future.

To evaluate spectral radiative properties, the absorption coefficient for soot aggregate is calculated from the Rayleigh solution (ref. 28) using the complex refractive index calculated from the Drude-Lorentz dispersion model and the parameter set of Habib and Vervisch (ref. 29). Scattering from soot particles is neglected at present to reduce computational time, but will be included in the future. The exponential-wide-band model of Edwards (ref. 30) is used to calculate the absorption coefficient for CO_2 and H_2O gases. The most accurate way to evaluate the total (i.e., across the spectral range) fluxes and divergence of flux is first to calculate them for each subdivided spectral range and then calculate the quadratures, but this is inefficient due to the large number of spectral subdivisions necessary to account for the steep variation of gas absorption coefficients and the number of iterations between the flame structure and the radiation solver. To focus on the convergence of iterations, we will test the Planck (a_P) and the Rossland (a_R) mean absorption coefficients given as (ref. 31)

$$a_P(T,P) = \frac{1}{\sigma T^4} \int_0^\infty a_\lambda(\lambda,T,P) e_{\lambda b}(\lambda,T) d\lambda \ , \text{ and } \ a_R(T,P) = \left[\int_0^\infty \frac{1}{a_\lambda(\lambda,T,P)} \frac{\partial e_{\lambda b}(\lambda,T)}{\partial e_b(T)} d\lambda \right]^{-1} . \quad (5)$$

In the future, we will examine other more sophisticated approaches.

Results and Discussions

We first compare the radiation heat transfer results from the YIX method based on true spectral integration (1 to 20 μm) and on both mean coefficients for a simulated turbulent ethylene diffusion flame. Fig. 1 shows a comparison of mixture spectral absorption coefficient against both means, and suggests that the Rossland mean should be reasonably accurate. Fig. 2 shows that the flux divergence based on the Rossland mean agrees quite well with that from integration. We thus base all subsequent "coupled" calculations on the Rossland mean coefficient.

We next compare the soot formation models by Moss et al. and by Khan et al. in Fig. 3(a) for flame temperature and in Fig. 3(b) for soot volume fraction, against experimental data for a laminar flame (ref. 32). From these figures, it is unclear which model is superior. However, calculations based on the experimental temperature, which is higher than predicted values around the centerline, reveal that Khan's model overpredicts the centerline volume fraction by a factor of 2, whereas Moss's changes only slightly. We therefore favor Moss's model at present. When we applied Moss's model with the same set of coefficients for the same fuel at different flow rates and compared with data, we found that the model is relatively insensitive to variations in fuel flow rate, and we will improve this in the future. Fig. 3(a) shows that the inclusion of radiative heat transfer provides a more accurate and correct trend in temperature profiles, when compared to those under adiabatic. Fig. 3(c) shows that the temperature converges smoothly in less than 10 iterations.

We then tested the model on normal gravity (1-g) and microgravity (0-g) laminar acetylene flames, for which we have measured soot volume fraction data for comparison. Fig. 4 shows comparisons between 1-g and 0-g for (a) measured soot volume fraction, (b) predicted soot volume fraction, and (c) predicted temperature. The dotted curves in temperature map are predicted flow streaklines, which also indicate the paths traversed by soot particles. Results in (b) and (c) were calculated using soot formation modeling coefficients slightly different from those for ethylene in Fig. (3). It is encouraging that the soot formation model is capable of accurately predicting the overall level and shape of the volume fraction distribution, especially since this is a smoking flame. It is also encouraging that the same 1-g soot modeling coefficients can be used to predict 0-g volume fraction with reasonable accuracy. Although the model predicts a wider soot shell than that measured for both 1-g and 0-g, it is expected that further adjustments in soot modeling coefficients will yield even better predictions.

Finally, we tested the model on turbulent ethylene flames, for which we should have measured data for comparison within a month or two. Fig. 5 shows a comparison of two predictions, one using the YIX solver and the other using the simple sink term model, against measured data for (a) volume fraction, and (b) temperature. Here, although it appears that the volume fraction results from the YIX solver are more accurate, the temperature results are roughly the same. Fig. 6 shows a comparison of 1-g and 0-g predictions for (a) volume fraction, and (b) temperature, using the same set of soot modeling coefficients and the YIX solver. Since this turbulent flame is momentum-dominant, the difference in flame shapes between 1-g and 0-g is not as substantial as that for the laminar flame in Fig. 4, which is more buoyancy-dominant.

In our future work, we will develop more accurate means of evaluating total radiative quantities, such as the wideband model used by Song and Viskanta (ref. 33). Their derivation of the "mean" radiative transfer equation to include turbulence-radiation effects is also worth noting. To investigate turbulence-radiation effects, we must also study the implementation of joint pdf (refs. 27 and 34) for correlating enthalpy, temperature, and mixture fraction. We will look for developments in turbulence-buoyancy interactions (ref. 15), which should be influential on 0-g flames.

References

1. M. G. Carvalho, F. Lockwood, and J. Taine (Eds.), Heat Transfer in Radiating and Combusting Systems, Springer-Verlag, Berlin-Heidelberg, 1991.
2. M. Y. Bahadori and R. B. Edelman, NASA CR-191109, 1993.
3. R. W. Bilger, Prog. Energy Comb. Sci., Vol. 1, 87-109, 1976.
4. S.-M. Jeng and G. M. Faeth, Vol. 106, 721-727, 1984.
5. J. P. Gore and G. M. Faeth, 21st Symp. (Int'l) Comb., 1521-1531, 1986.
6. F. C. Lockwood and A. S. Naguib, Comb. Flame, Vol. 24, 109-124, 1975.
7. G. M. Faeth, S.-M. Jeng, and J. Gore, ASME HTD-Vol. 45 Heat Transfer in Fire and Comb. Systems, 137-151, 1985.

8. J.-Y. Chen, W. Kollmann, and R. W. Dibble, 18th Annual Pittsburgh Conf. Modeling and Simulation, 1987.
9. W. C. Reynolds, Department of Mechanical Engineering, Stanford University, 1986.
10. R. W. Bilger, Comb. Flame, Vol. 30, 277-284, 1977.
11. C. N. Peters and B. Rogg (Eds.), Reduced Kinetic Mechanisms for Applications in Combustion Systems, Springer-Verlag, Berlin-Heidelberg, 1993.
12. K. J. Syed, C. D. Stewart, and J. B. Moss, 23rd Symp. (Int'l) Comb., 1533-1541, 1990.
13. J. B. Moss, C. D. Stewart, and K. J. Syed, 22nd Symp. (Int'l) Comb., 413-423, 1988.
14. K. M. Leung, R. P. Lindstedt, and W. P. Jones, Comb. Flame, Vol. 87, 289-305, 1991.
15. M. Fairweather, W. P. Jones, and R. P. Lindstedt, Comb. Flame, Vol. 89, 45-63, 1992.
16. L. Tong, Ph. D. Dissertation, Wayne State University, expected May 1995.
17. I. M. Khan, G. Greeves, and D. M. Probert, Institution of Mechanical Engineers, p. 205, 1971.
18. I. M. Khan and G. Greeves, Chapter 25 in Heat Transfer in Flames, Afgan and Beer, Eds., Scripta Book Co, 1974.
19. K. B. Lee, M. W. Thring, and J. M. Beer, Comb. Flame, Vol. 6, 137-145, 1962.
20. T. W. Tong and R. D. Skocypec, Developments in Radiative Heat Transfer, S. T. Thynell et al., Eds., ASME HTD-Vol. 203, 235-264, 1992.
21. Z. Tan and J. R. Howell, J. Thermophys. Heat Transfer, Vol. 4, 419-424, 1990.
22. P.-F. Hsu, Z. Tan, and J. R. Howell, J. Thermophys. Heat Transfer, Vol. 7, 487-495, 1993.
23. P.-F. Hsu and J. C. Ku, J. Thermophys. Heat Transfer, Vol. 8, 434-440, 1994.
24. P.-F. Hsu and J. C. Ku, submitted to ICHMT Int'l. Symp. Radiative Transfer, 1995.
25. J. H. Kent and D. Honnery, Comb. Sci. Tech., Vol. 54, 383-397, 1987.
26. M. P. Menguc and R. Viskanta, J. Heat Transfer, Vol. 108, 271-276, 1986.
27. J. P. Gore, U.-S. Ip, and Y. R. Sivathanu, J. Heat Transfer, Vol. 114, 487-493, 1992.
28. J. C. Ku and K.-H. Shim, J. Heat Transfer, Vol. 113, 953-958, 1991.
29. Z. G. Habib and P. Vervisch, Comb. Sci. Tech., Vol. 59, 261-274, 1988.
30. D. K. Edwards, Advances in Heat Transfer, Vol. 12, T. F. Irvine, Jr. and J. P. Harnett, Eds., Academic Press, New York, 115-193, 1976.
31. R. Siegel and J. R. Howell, Thermal Radiation Heat Transfer, 3rd ed., Hemisphere, Washington, DC, 1992.
32. R. J. Santoro, T. T. Yeh, J. J. Horvath, and H. C. Semerjian, Comb. Sci. Tech., Vol. 53, 89-115, 1987.
33. T. H. Song and R. Viskanta, J. Thermophys. Heat Transfer, Vol. 1, 56-62, 1987.
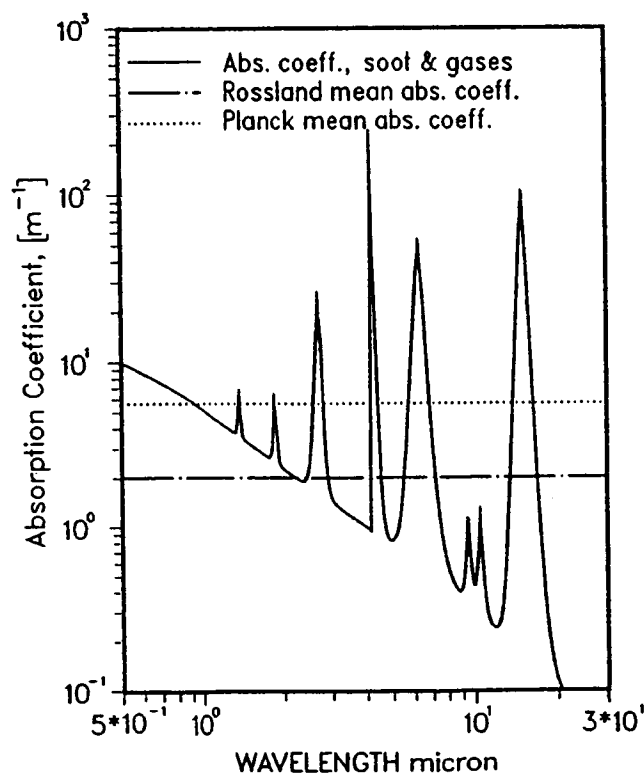34. J. Janicka and W. Kollmann, 17th Symp. (Int'l) Comb, 421-430, 1978.

Fig. 1 Absorption coefficients for a soot and gases mixture at 1400K, with 0.1 mole fraction for CO_2 and H_2O, and a soot volume fraction of 10^{-6}.
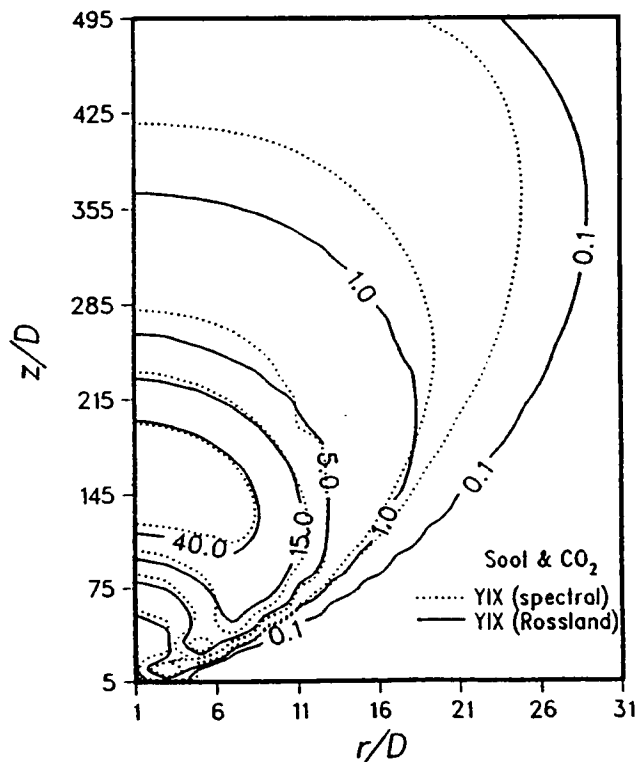

Fig. 2 The divergence of flux contours for a simulated ethylene diffusion flame (D = 0.58 mm, $\dot{Q}$ = 3.96 cm³/sec, and Re = 536).

(a) Flame Temperature   (b) Soot Volume Fraction   (c) Convergence of Temperature
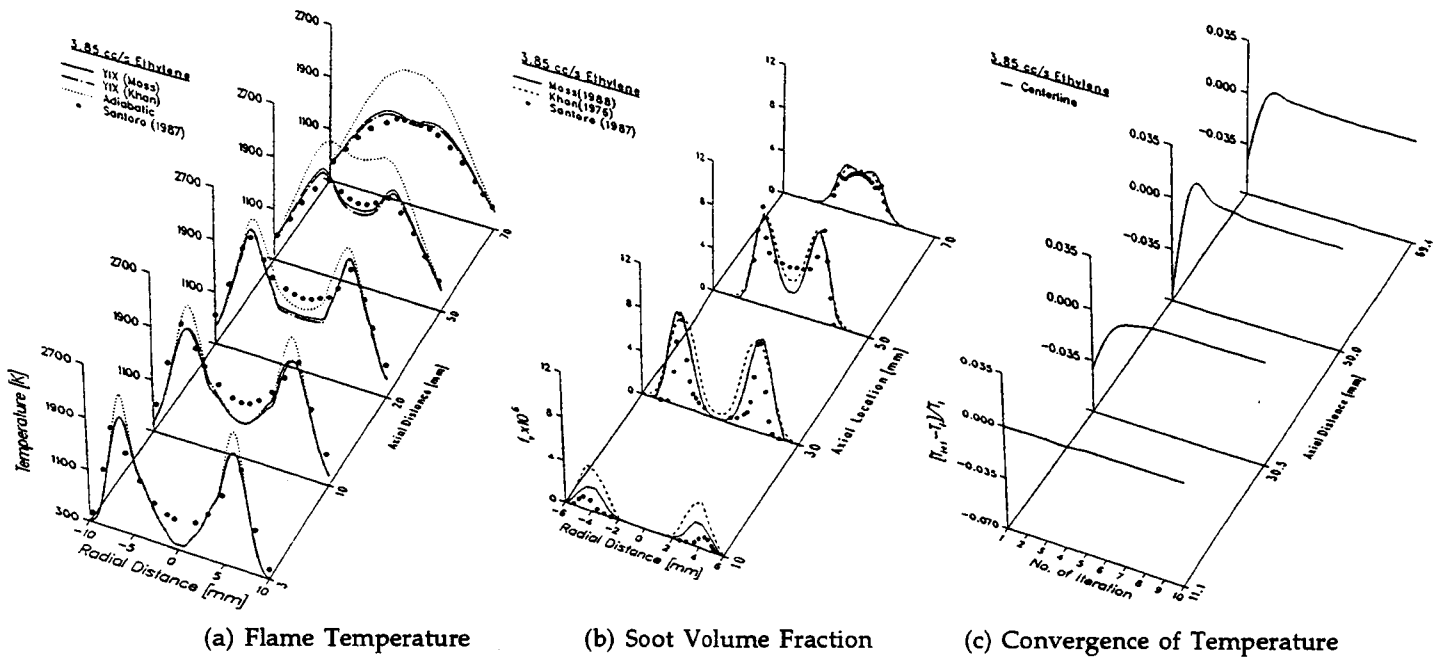
Fig. 3 Comparisons of model predictions to experimental data, and the trend of convergence of temperature during iterations between the structure and the radiation solver, for a laminar ethylene co-flow diffusion flame (ref. 32).
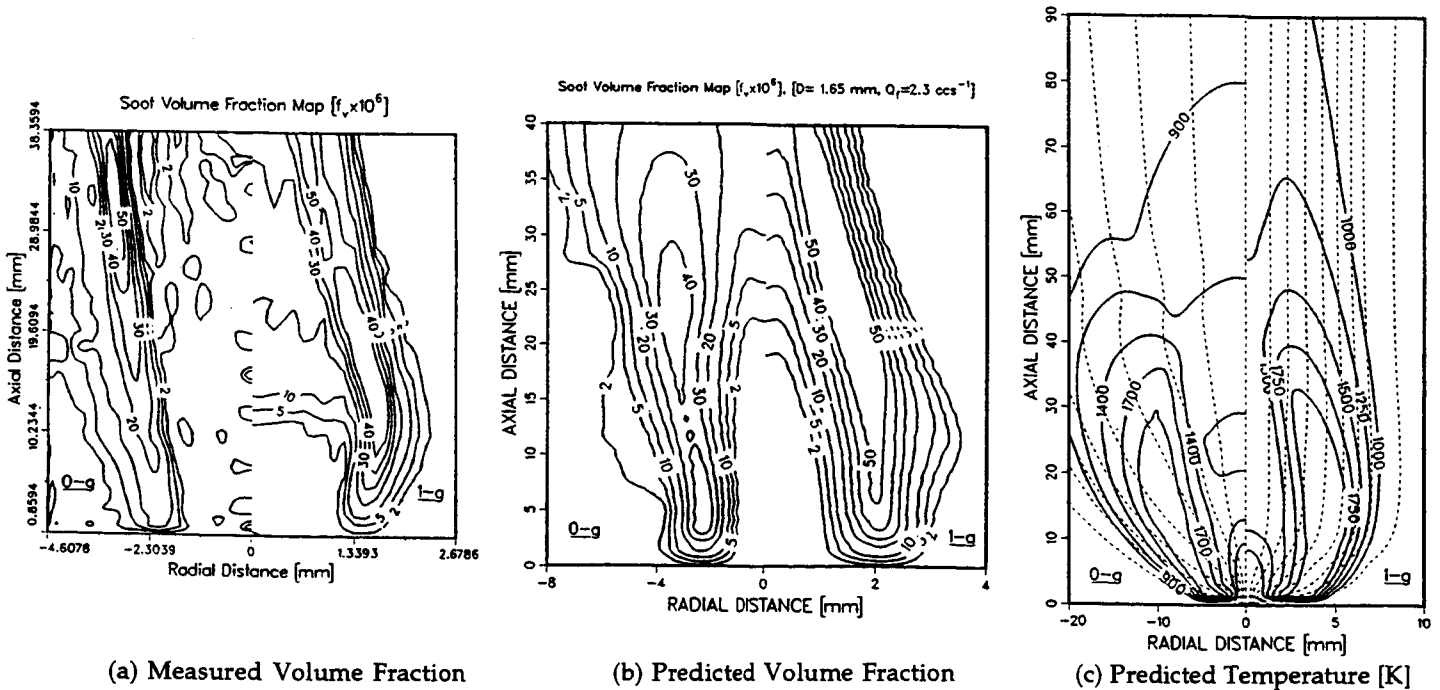

(a) Measured Volume Fraction   (b) Predicted Volume Fraction   (c) Predicted Temperature [K]

Fig. 4 Comparisons of model predictions to experimental data for a laminar acetylene jet diffusion flame.
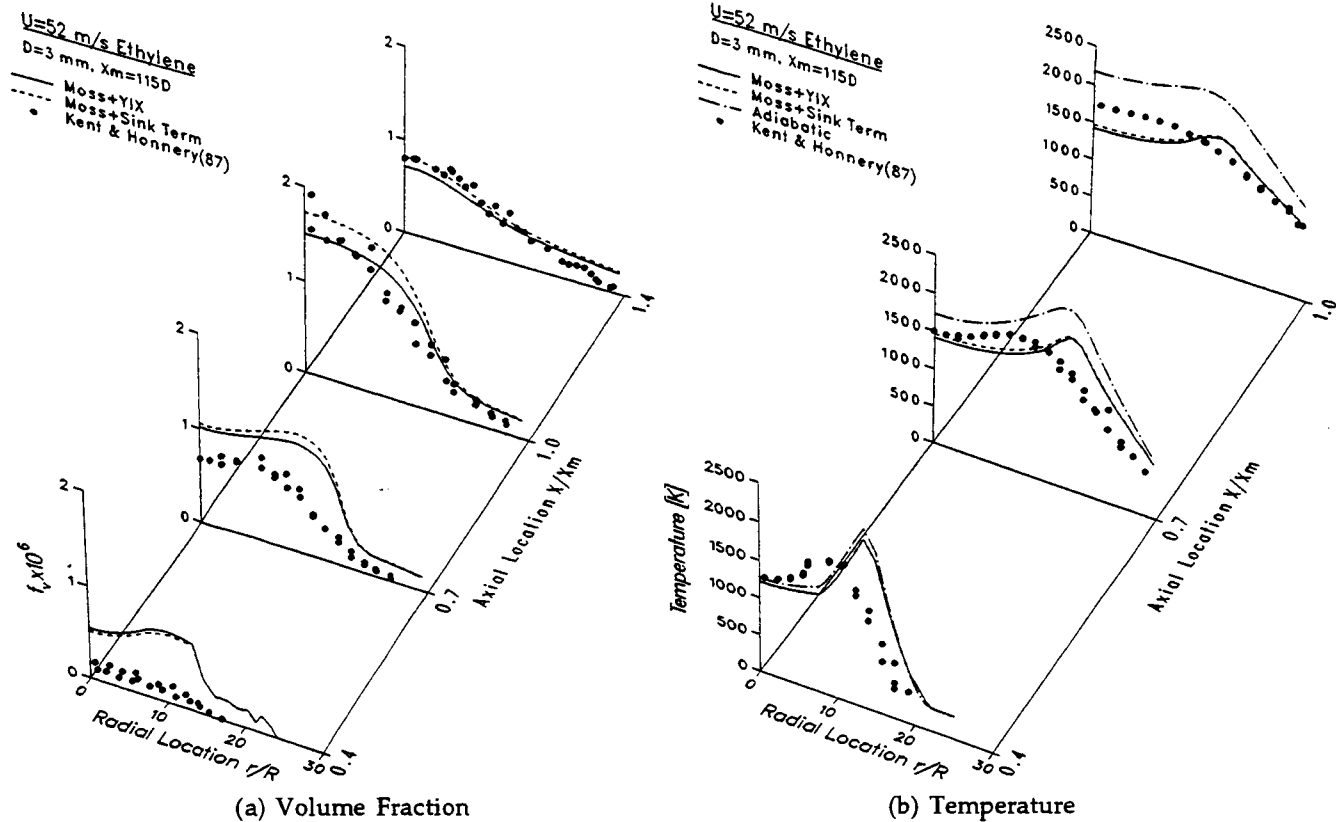
379

(a) Volume Fraction

(b) Temperature

Fig. 5 Comparisons of model predictions to experimental data for a 1-g turbulent ethylene jet diffusion flame.
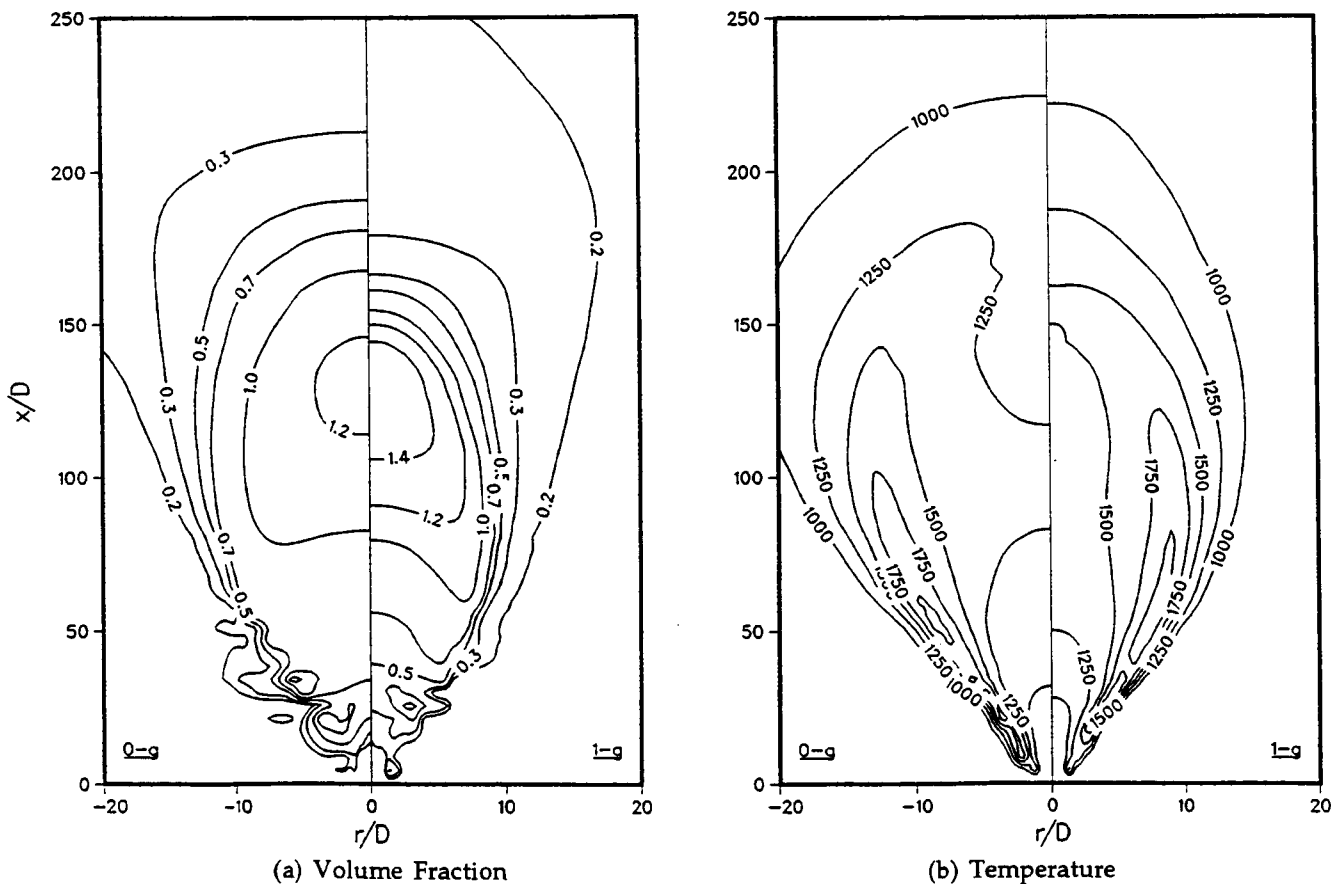

(a) Volume Fraction

(b) Temperature

Fig. 6 Predictions for 1-g and 0-g turbulent ethylene jet diffusion flames (D = 3 mm, V = 52 m/s, and Re = 9.62X10^3).

380